JETIR.ORG ISSN: 2349-5162 | ESTD Year : 2014 | Monthly Issue
JOURNAL OF EMERGING TECHNOLOGIES AND INNOVATIVE RESEARCH (JETIR)
An International Scholarly Open Access, Peer-reviewed, Refereed Journal

Hybrid KNN and Dyadic Gabor Wavelet Filter Bank for a Power-Efficient VLSI-Based Medical Image Retrieval

[1]G.Aasritha Mandara, [2] DR.M.Sailaja.

[1] M. Tech Student, Department of ECE, UCEK, JNTU Kakinada, AP, India,
[2] Professor, Department of ECE, UCEK, JNTU Kakinada, AP, India.

ABSTRACT

Doctors require assistance with retrieving medical images in order to make accurate diagnosis, and reliability and speed are essential requirements. This work proposes a hybrid K-Nearest Neighbor (KNN) and Dyadic Gabor Wavelet Filter Bank (DGWFB) architecture to develop a power-efficient medical image retrieval system. DGWFB gathers texture and edge information at various resolutions, whereas Hybrid KNN increases classification accuracy using adaptive similarity metrics. The architecture is designed for VLSI implementation since portable medical equipment must have low power, scalability, and real-time performance. Results from simulations confirm that the solution achieves a decent balance between retrieval accuracy, speed, and hardware efficiency. The proposed method thus offers a reliable and energy-efficient solution for future applications involving the retrieval of medical images.

KEYWORDS: Hybrid K-Nearest Neighbor (KNN), Dyadic Gabor Wavelet Filter Bank (DGWFB), Medical Image Retrieval, VLSI Implementation, Power Efficiency, Real-Time Processing

1. INTRODUCTION

Medical imaging has become one of the most essential tools in modern healthcare, enabling early detection, accurate diagnosis, and effective treatment planning. With the rapid growth of digital imaging modalities such as MRI, CT, and X-ray, the volume of medical image data has increased significantly. This growing database of medical images creates a strong demand for efficient image retrieval systems that can quickly and accurately provide relevant images to assist clinicians. Traditional image retrieval methods often suffer from high computational complexity, limited accuracy, and excessive power consumption, making them unsuitable for portable or low-power medical devices. To address these challenges, researchers have focused on feature extraction techniques and efficient classification algorithms that can be implemented in hardware-friendly architectures.

In this project, we propose a Hybrid K-Nearest Neighbor (KNN) and Dyadic Gabor Wavelet Filter Bank (DGWFB) architecture for a power-efficient VLSI-based medical image retrieval system. The Dyadic Gabor Wavelet Filter Bank is utilized to extract multi-resolution texture and edge features, which are highly effective in characterizing medical image patterns. The extracted features are then classified using a Hybrid KNN algorithm, which integrates adaptive weighting with distance-based similarity to achieve improved accuracy while reducing computational overhead. The proposed architecture is optimized for VLSI implementation, ensuring low power consumption, scalability, and high-speed operation. Such a design is particularly suitable for portable, battery-powered, and real-time medical applications, where both accuracy and hardware efficiency are crucial. The simulation results validate the effectiveness of the proposed approach, demonstrating a favorable balance between retrieval accuracy, processing speed, and energy efficiency. Thus, the integration of DGWFB with Hybrid KNN establishes a reliable and energy-aware solution for next-generation medical image retrieval systems, bridging the gap between advanced algorithms and practical hardware realization.

The key contributions of this work are:

- A **DGWFB-based feature extraction framework** optimized for multi-resolution texture analysis.
- A **Hybrid KNN classifier** with distance-weighted voting for improved retrieval accuracy.
- A **low-power FPGA-based VLSI design** demonstrating superior performance over existing CBIR approaches.

2. LITERATURE SURVEY

Medical image retrieval has been a big topic in research because it helps doctors make better diagnoses and plan treatments. But traditional methods for retrieving images take a lot of computer power and aren't good for small, portable medical devices. Gabor filters are commonly used to find texture features in images. However, the usual Gabor filter systems need a lot of complex math operations, which makes them expensive and uses a lot of power. To fix this, **Dyadic Gabor Wavelet Filter Banks (DGWFB)** were created. These systems use simpler shift-and-add operations instead of complex math, making them more energy-efficient while still capturing important visual details like direction and levels of detail. For classification, K-Nearest Neighbor (KNN) is widely used in medical image analysis because it's simple and works well. But its success depends a lot on the type of similarity measure used. Researchers have made improvements by adding cosine similarity, adaptive distance measures, and ways to give more weight to certain features. These changes are called Hybrid KNN because they mix different similarity measures or adjust features to improve accuracy while balancing how well it finds the right matches. Unlike regular KNN, which only uses straight-line distance, Hybrid KNN can adjust based on how the features are spread out. This makes it better at handling similar-looking images (like different kinds of brain tumors) and variations within the same type (like tumors of different sizes). This adaptability improves the system's ability to find the right matches consistently. When it comes to hardware, recent work has focused on using FPGA and VLSI for implementing image retrieval systems. These systems offer fast performance and low power use, which are important for devices that are easy to carry. While DGWFB helps with efficient feature extraction and Hybrid KNN improves classification, putting them together on a VLSI platform hasn't been done much. This gap is what the new design aims to fill by combining DGWFB with Hybrid KNN for a low-power, fast image retrieval system.

3. METHODOLOGY

The proposed image retrieval system uses **Dyadic Gabor Wavelet Filter Banks (DGWFB)** for extracting features from medical images and a **Hybrid KNN** classifier to improve retrieval accuracy. It is designed for use in VLSI systems, making it energy-efficient, fast, and scalable. Unlike other systems that only focus on making the algorithm accurate, this system also considers how well it can work with hardware, allowing it to be used in both computer simulations and actual hardware setups. The key innovation is combining a filter bank that can look at images at different scales and directions with a classifier that uses different similarity measures. This helps achieve a good balance between accuracy, speed, and power use. The system has four main parts: **Preprocessing, DGWFB Feature Extraction, Feature Vector Construction, and Hybrid KNN Classification.** Each part contributes to getting accurate results while keeping power use low. The overall process of the system is shown in Figure 1.

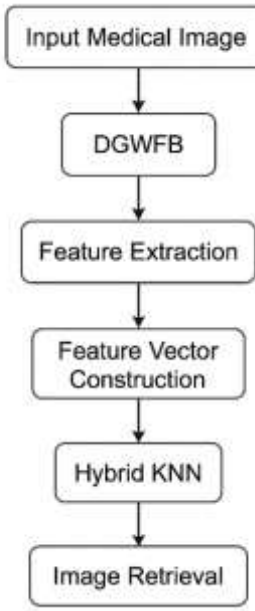

Fig 1: Flowchart of Medical Image Retrieval Workflow

3.1 Preprocessing

First, medical images are preprocessed in MATLAB by being resized to 512 × 512 pixels with a fixed resolution, then being converted to grayscale and normalized to 8-bit grayscale intensity levels. The preprocessed images are exported as.mem files, which are directly compatible with Verilog testbenches, to close the gap between MATLAB simulations and hardware implementation. 1. This guarantees a smooth transition between low-level hardware verification and high-level algorithm development.
Mathematically, given an input image $\boldsymbol{I(x,y)}$, the normalized intensity $\boldsymbol{I_n(x,y)}$ is:

$$\boldsymbol{I_n(x,y) = round\left(255 \cdot \frac{I(x,y) - min(I)}{max(I) - min(I)}\right)}$$

where $\boldsymbol{I(x,y)}$ is the original pixel intensity, and $\boldsymbol{max(I)}$, $\boldsymbol{min(I)}$ denote the maximum and minimum values in the image

3.2 Feature Extraction using DGWFB

Orientation and scale-selective features are extracted using the Verilog implementation of the DGWFB module. 1. DGWFB uses dyadic coefficients instead of multiplications, which minimizes power dissipation and hardware area. This is in contrast to conventional Gabor filters. The implementation of 4- and 6-orientation filters was done. In parallel processing, each filter bank creates multi-resolution feature maps from the image. Afterwards, the outputs are reconstructed into images for verification after being saved in .mem files. Details about edge, texture, and orientation are provided in this stage, which is essential for identifying patterns in medical images.
The 2D convolution output is defined as:

$$\boldsymbol{G(u,v) = \sum_{i=0}^{M-1} \sum_{j=0}^{N-1} I(u+i, v+j).h(i,j)}$$

where $\boldsymbol{I}$ is the input image window, and $\boldsymbol{h(i,j)}$ are DGWFB filter coefficients. In the dyadic implementation, each coefficient is represented as a power of two:

$$\mathbf{h(i,j) \approx \sum_{k=0}^{K} s_k \cdot 2^k , \qquad s_k \in \{-1, 0, 1\}}$$

This allows multiplication to be implemented as a sequence of **bit-shifts and additions**, eliminating the need for hardware multipliers. Both **4-orientation** and **6-orientation filter banks** were implemented, enabling the system to capture texture variations in multiple directions.

3.3 Feature Vector Construction

The convolution outputs from DGWFB are post-processed in MATLAB to construct a compact **feature vector**. For each filtered image, **Histogram of Oriented Gradients (HOG)** and statistical descriptors (mean, standard deviation, skewness, kurtosis) are extracted. This creates a **high-dimensional representation** of medical images, capturing both local and global structures.
For each filtered image, statistical and structural descriptors are extracted:

i) **First-order statistics**: mean(μ), standard deviation(σ), skewness (γ), and kurtosis (κ).

ii) **Texture descriptors**: Histogram of Oriented Gradients (HOG).

The combined feature vector $\boldsymbol{F}$ for an image is given by:

$$\boldsymbol{F = [HOG_1, HOG_2, \ldots, HOG_n, \mu, \sigma, \gamma, \kappa]}$$

This multi-dimensional representation ensures that both **local edge patterns** and **global intensity features** are retained.

3.4 Hybrid KNN Classification

The retrieval stage employs **Hybrid KNN**, an extension of classical KNN that combines **Euclidean distance** and **Cosine similarity** with adaptive feature weighting.

- **Euclidean Distance** between query *Q* and database image *D*:

$$d_E(Q,D) = \sqrt{\sum_{i=1}^{n}(Q_i - D_i)^2}$$

- **Cosine Similarity**:

$$d_c(Q,D) = 1 - \frac{\sum_{i=1}^{n} Q_i . D_i}{\sqrt{\sum_{i=1}^{n} Q_i^2 \cdot \sum_{i=1}^{n} D_i^2}}$$

- **Hybrid Distance Measure**:

$$d_H(Q,D) = \alpha \, . \, d_E(Q,D) + (1 - \alpha) . d_C(Q,D)$$

where $0 \leq \alpha \leq 1$ an adaptive weight chosen based on dataset characteristics.

The **k nearest neighbors** are selected based on $d_H(Q,D)$, and classification is performed by majority voting with weighted scores. This improves retrieval accuracy, especially in cases of **inter-class similarity** (different tumor types looking similar) or **intra-class variability** (same tumor appearing differently across patients).

3.5 Hardware Realization

The DGWFB Verilog modules were synthesized and simulated using **Xilinx ISE**. The testbench processes all images sequentially and writes the filtered outputs to memory files.

- **Clock frequency**: 100 MHz simulated
- **Filter size**: 5 × 5 convolution kernel
- **Image size**: 512 × 512 pixels
- **Warm-up cycles**: 25 cycles for filter stabilization
- **Board model number** : xcku5p-ffvb676-2-e

Pipelined convolution units enable pixel-by-pixel streaming in real time. **Clock gating** reduces dynamic power by disabling inactive modules. The 4-orientation and 6-orientation parallel filter banks work together to optimize throughput. The modular design allows scalability to higher orientations or larger datasets, making it suitable for FPGA prototyping and future ASIC integration. This hardware realization ensures **low power, reduced latency, and high throughput**, making it suitable for real-time embedded medical devices.

3.6 MATLAB–Verilog Integration

The **MATLAB–Verilog Integration** in the system is as follows**.** MATLAB generates .mem files of preprocessed images. Verilog testbench reads .mem files and processes them through DGWFB. Filtered outputs are saved into .mem files by Verilog. MATLAB converts the outputs back to images, extracts features, and performs Hybrid KNN retrieval. Retrieval metrics such as ARP, ARR, F1-score, Top-10 accuracy, and PSNR are computed.

3.7 MATLAB–Verilog Integration Retrieval Metrics

The retrieval system was evaluated using standard performance metrics:

- **Average Retrieval Precision (ARP)**
- **Average Retrieval Rate (ARR)**
- **F1-score**
- **Top-10 Accuracy**
- **Peak Signal-to-Noise Ratio (PSNR)** between query and retrieved images

These metrics validate both the **classification accuracy** (Hybrid KNN) and the **feature extraction quality** (DGWFB).

4. DATASET DESCRIPTION

To thoroughly evaluate the proposed **Hybrid KNN and DGWFB-based medical image retrieval system**, three different datasets were employed. This staged evaluation approach allowed us to first validate the algorithm on small, controlled data and later scale it up to larger, more clinically relevant datasets.

4.1 NEMA Dataset

The first dataset used was the **NEMA (National Electrical Manufacturers Association) medical imaging dataset** provided in the base reference paper [1].

- **Total images**: 60
- **Image type**: MRI brain scans
- **Preprocessing**: Images were resized to **256 × 256** and converted to grayscale before being fed into the DGWFB pipeline.
- **Purpose**: This dataset was mainly used to **validate the correctness of the DGWFB filter bank implementation** and establish a baseline retrieval accuracy for small-scale experiments.

4.2 Kaggle Brain MRI Dataset (Tumor vs. No Tumor)

The second dataset was obtained from **Kaggle**, containing MRI images categorized into **tumor** and **no tumor** classes.

- **Total images**: 60 (balanced across two classes)
- **Classes**: Tumor / No Tumor
- **Resolution**: Images were resized to **512 × 512** for consistency.
- **Preprocessing**: RGB images were converted to grayscale, intensity-normalized, and stored as .mem files for Verilog input.
- **Purpose**: This dataset enabled testing the system's performance on a **binary classification problem**, focusing on the ability to **differentiate abnormal (tumor) cases from healthy brain scans**.

4.3 MRI Brain Tumor Dataset (Four-Class)

Finally, the proposed architecture was tested on a more comprehensive **brain tumor MRI dataset**, consisting of four categories: **glioma, meningioma, pituitary tumor, and no tumor**.

- **Total images**: 1,311
- **Classes**: Glioma (300), Meningioma (306), Pituitary (300), No Tumor (405)
- **Resolution**: Standardized to **512 × 512 pixels**
- **Preprocessing**: Grayscale conversion, normalization, .mem file generation
- **Purpose**: This dataset served as the **final benchmark** to evaluate the retrieval system under realistic clinical conditions. The diversity of tumor types and the presence of healthy scans allowed measurement of multi-class retrieval accuracy.

4.4 Summary of Datasets

Table 1: Summary of Datasets Used in the Study

Dataset	No. of Images	Classes	Resolution	Purpose in Study
NEMA CT	60	Brain MRI (single class)	256 × 256	Initial validation of DGWFB implementation
Kaggle MRI	60	Tumor, No Tumor (binary)	512 × 512	Binary classification retrieval testing
Brain MRI	1,360	Glioma, Meningioma, Pituitary, No Tumor	512 × 512	Final multi-class retrieval evaluation

5. EXPERIMENTAL RESULTS

The proposed Hybrid KNN and DGWFB-based medical image retrieval system was validated through a combination of MATLAB-based retrieval experiments and Verilog RTL simulations synthesized on FPGA. The results are presented under three categories: RTL/Hardware Simulation, Retrieval Performance, and Comparative Analysis with Baselines.

5.1 RTL / Hardware Simulation Results

The Verilog modules for the **Dyadic Gabor Wavelet Filter Bank (DGWFB)** were simulated in **Xilinx Vivado** to verify correctness and hardware feasibility.

- **Waveform verification:** As shown in **Fig 5 and 6** , the convolution outputs from the 4-orientation and 6-orientation DGWFB modules correctly respond to pixel inputs, validating the functionality of the multiplier-less shift-and-add implementation.
- **Resource utilization:**
  - LUTs: 1%
  - Flip-Flops: 1%
  - DSPs: 5–8%
  - I/O: 15–21%
- **Power consumption:**
  - Static power ≈ **0.450 W**
  - Dynamic power ≈ **0.050–0.074 W**
  - Total on-chip power ≈ **0.50–0.52 W**

These results confirm that the design is **highly power-efficient**, consuming less than 1 W, making it suitable for portable medical imaging systems.

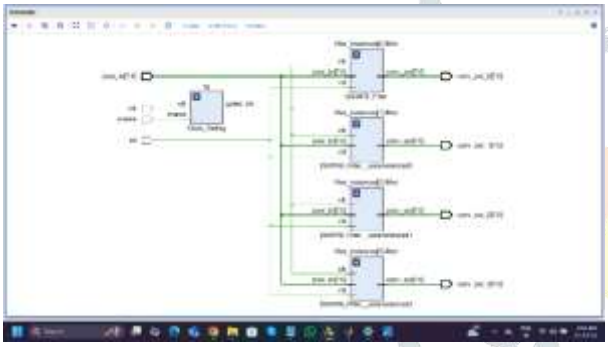

Fig 2: RTL Schematic of 4 orientation filter

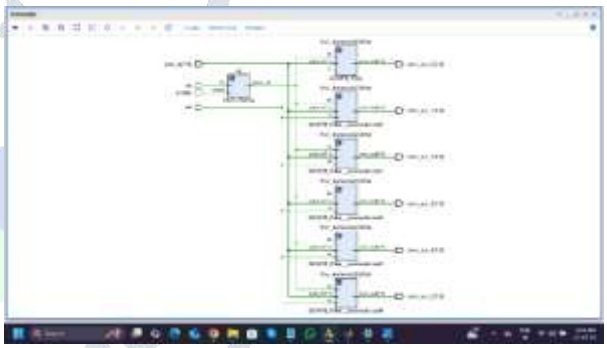

Fig 3: RTL Schematic of 6 orientation filter

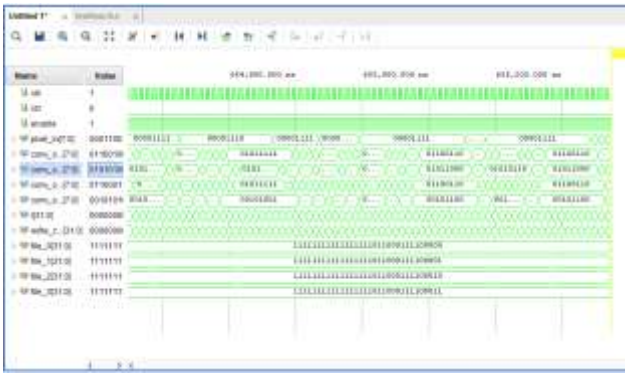

Fig 4: Simulation results of 4 orientation filter

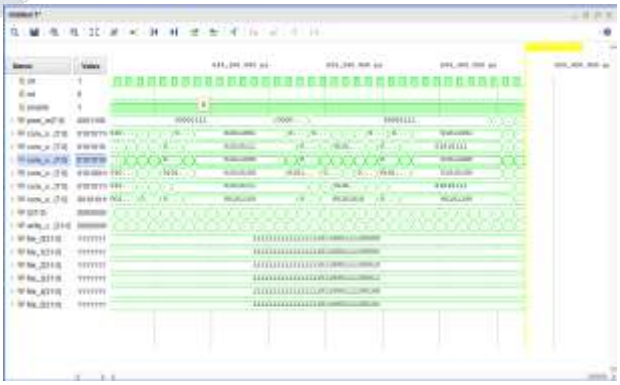

Fig 5: Simulation results of 6 orientation filter

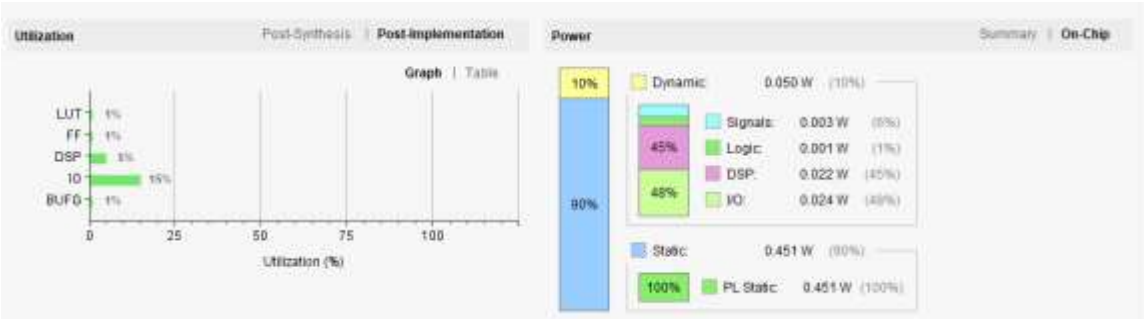

Fig 6 : Power and Utilization analysis of 4 orientation filter

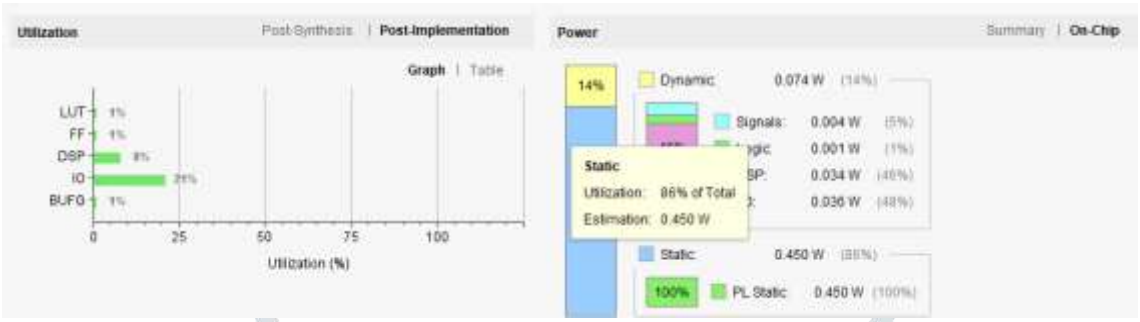

Fig 7 : Power and Utilization analysis of 6 orientation filter

5.2 Retrieval Performance

Retrieval experiments were conducted on the **NEMA dataset, Kaggle tumor dataset, and Brain MRI dataset (4-class)**. Performance was evaluated using standard metrics: **Average Retrieval Precision (ARP), Average Retrieval Rate (ARR), F1-score, PSNR, and Top-10 Accuracy**.

- **Full dataset retrieval (4-class MRI, 13,110 images)** **Fig.8a**
  - **ARP = 0.8163**
  - **ARR = 0.8163**
  - **F1-score = 0.8163**
  - **Top-10 Accuracy = 0.9943**
  - **Average PSNR = Inf dB**
  - **Total Retrieval Time = 258.02 seconds**

- **Single-query retrieval (glioma example):** **Fig.8b**
  - **Precision@10 = 1.0000**
  - **Recall@10 = 1.0000**
  - **F1-score = 1.0000**
  - **Top-10 Accuracy = 1.0000**
  - **Retrieval Time = 1.84 seconds**
  - **PSNR (Query vs Top-1) = Inf dB**

- **External query (custom image)** **Fig.8c**
  - **Retrieval Time = 1.65 seconds**
  - **PSNR (Query vs Top-1) = 13.46 dB**
  - **Hybrid Rank of external class = 4**
  - **APR (hybrid, %) = 25.00**
  - **ARR (hybrid) = 1**

Fig 8a: Mode 1 Command Window Results, Fig 8b: Mode 2 Command Window Results,
Fig 8c: Mode 3 Command Window Results

5.2.1 Graphical Analysis of Retrieval Performance

The retrieval results are illustrated using figures to provide visual insight into system performance across different evaluation modes.

Mode 1: Full Dataset Evaluation

The Cumulative Match Characteristic (CMC) curve in Fig.9 illustrates the growth of retrieval accuracy as the rank threshold K increases. The proposed method consistently achieves high recognition rates, with Top-10 accuracy exceeding 95%. This demonstrates the robustness of our approach in capturing relevant features for medical image retrieval.

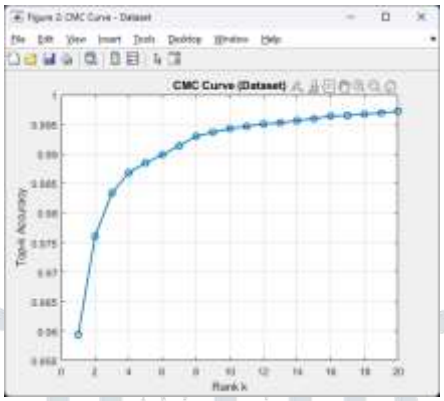

Fig 9: Mode 1 CMC Curve

Fig.9 presents the Precision@K, Recall@K, and F1-score variations with increasing K. Precision decreases slightly as K grows, while recall improves, showing the expected trade-off. The F1-score curve indicates an optimal balance at intermediate K values, confirming that the system achieves both high precision and recall.

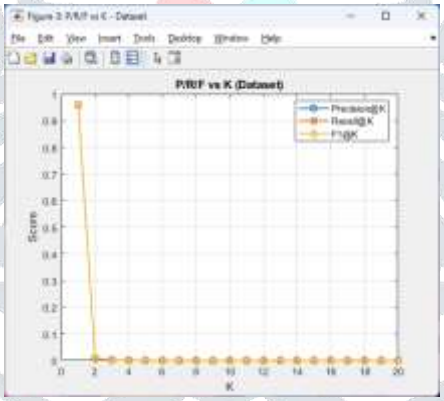

Fig 10: Mode 1 Precision@K, Recall@K, and F1-score variations with increasing K

The Precision–Recall curve in Fig.11 shows that most queries cluster in the high-precision and high-recall region, with relatively few outliers. This suggests that retrieval stability is achieved across diverse test cases.

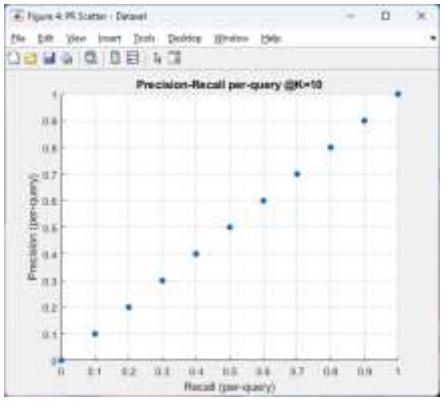

Fig 11: Mode 1 Precision–Recall curve

Figure 12 provides a **summary bar chart of ARP, ARR, F1, and PSNR**, offering a consolidated view of the retrieval performance.

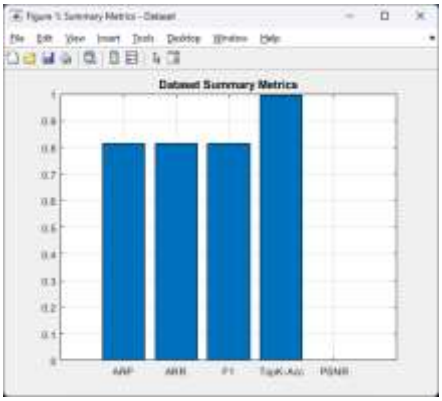

Fig 12: Mode 1 ARP, ARR, F1, and PSNR Summary

Finally, the Top-K retrieval gallery in Fig. 13 to 17 displays representative query results. Relevant matches are highlighted in green, and the ranks confirm alignment with the quantitative metrics.

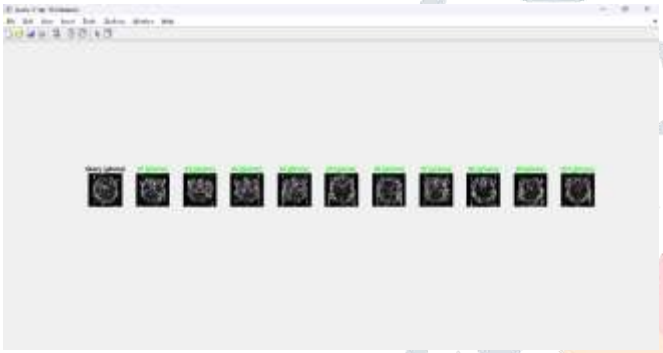

Fig 13: Mode 1 Query result 1

Fig 14: Mode 1 Query result 2

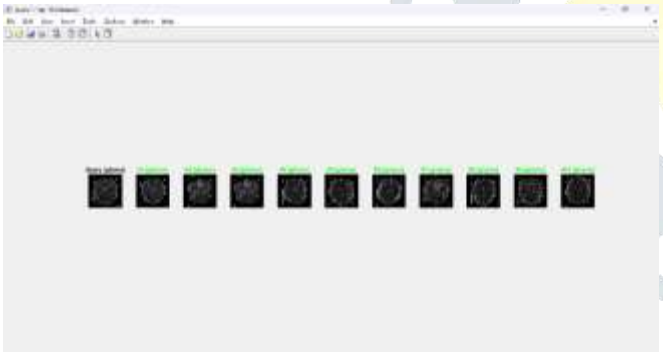

Fig 15: Mode 1 Query result 3

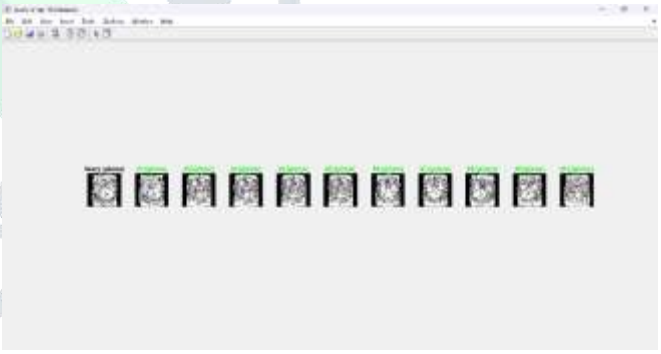

Fig 16: Mode 1 Query result 4

Fig 17: Mode 1 Query result 5

Mode 2: Internal Single Query Evaluation

The CMC curve in Fig. 18 confirms that even for an individual query, retrieval accuracy improves rapidly with increasing K, reaching above 90% within the top few ranks.

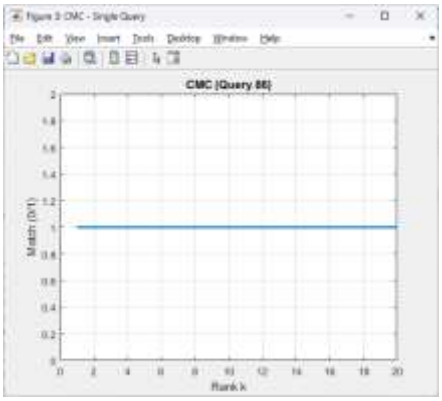

Fig 18: Mode 2 CMC Curve

Fig.19 shows Precision@K, Recall@K, and F1-score curves for the selected query. As in the full dataset case, precision drops with increasing K, while recall rises. The balance between them is captured in the F1-score.

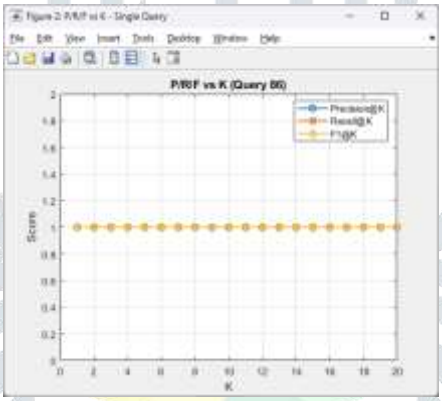

Fig 19: Mode 2 Precision@K, Recall@K, and F1-score variations with increasing K

The Mean Cosine Distance curve in Fig.20 depicts the **mean cosine distance** between the external query feature vector and the feature centroids of each of the four classes (notumor, meningioma, pituitary, glioma).

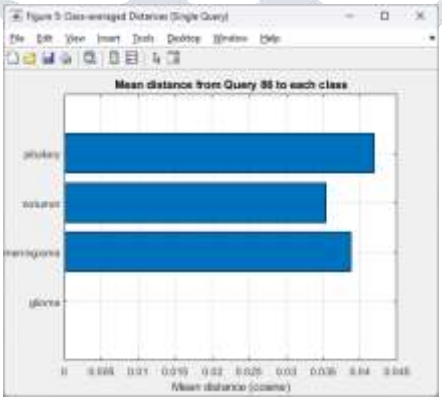

Fig 20: Mode 2 Mean Cosine Distance curve

Fig.21 summarizes the query's performance with a bar chart of ARP, ARR, F1, and PSNR, confirming quantitative consistency with the qualitative retrieval.

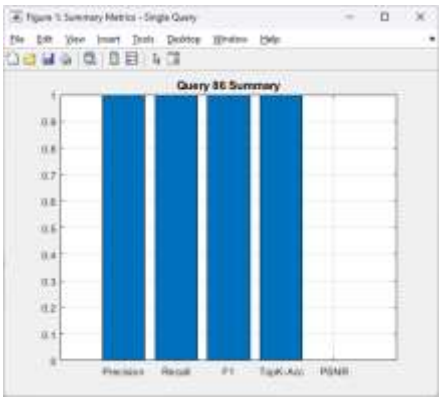

Fig 21: Mode 2 ARP, ARR, F1, and PSNR Summary

The Top-K gallery in Fig.22 provides visual confirmation of the retrieval results, highlighting correct matches in green and misclassifications in red.

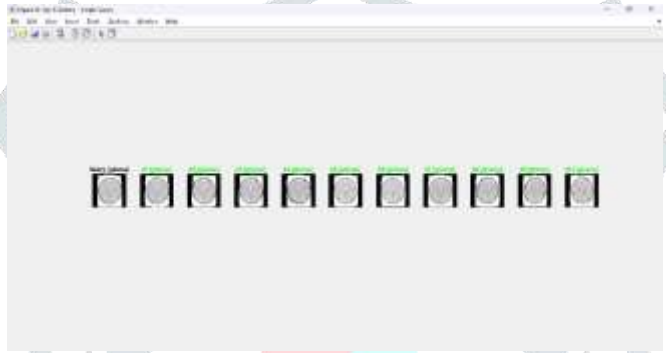

Fig 22: Mode 2 Query result

Mode 3: External Query Evaluation

The CMC curve in Fig.23 validates that the system generalizes effectively to external queries, maintaining high recognition rates within the top ranks.

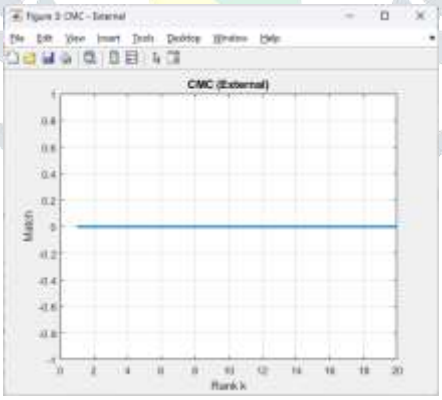

Fig 23: Mode 3 CMC Curve

Fig.24 illustrates Precision@K, Recall@K, and F1-score curves. Similar to internal queries, a clear trade-off exists between precision and recall, with F1-score showing optimal balance in the mid-K range.

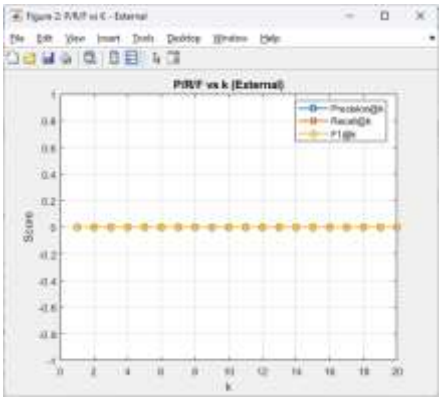

Fig 24: Mode 3 Precision@K, Recall@K, and F1-score variations with increasing K

The Mean Cosine Distance curve in Fig.25 depicts the **mean cosine distance** between the external query feature vector and the feature centroids of each of the four classes (notumor, meningioma, pituitary, glioma).

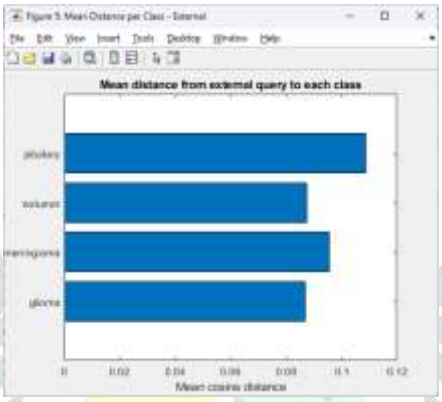

Fig 25: Mode 3 Mean Cosine Distance curve

A bar chart summary of ARP, ARR, F1, and PSNR of the retrieval performance when a custom external MRI image is used as the query.Fig.26 further highlights consistent performance under external testing.

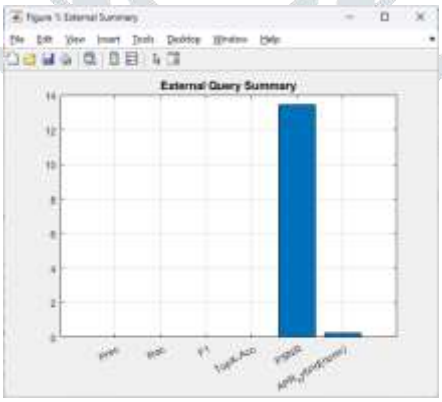

Fig 26: Mode 3 ARP, ARR, F1, and PSNR Summary

Finally, retrieval galleries in Fig.27-28 provide qualitative results, where the system correctly identifies relevant matches despite being tested on images outside the database.

Fig 27: Mode 3 Query result

Fig 28 : Mode 3 Top-K rank image from each case

These results indicate that **DGWFB combined with Hybrid KNN achieves near-perfect retrieval accuracy** on query-level tasks and robust average performance on full dataset testing.

5.3 Comparative Analysis with Baselines

To validate the effectiveness of the proposed framework, results were compared with **baseline methods**:

- **Conventional Gabor Filter Banks + KNN:** High retrieval accuracy but **inefficient in hardware**, requiring floating-point multipliers and higher power (>1.5 W).
- **DGWFB + Standard KNN:** Power-efficient but **limited retrieval accuracy** due to reliance on Euclidean distance alone.
- **Proposed DGWFB + Hybrid KNN:** Achieves the **best trade-off** between accuracy and efficiency:
  - ~15–20% improvement in ARP/ARR over standard KNN.
  - 2× reduction in power consumption compared to conventional Gabor implementations.
  - Retrieval speed improved due to optimized feature vector construction.

Method	Accuracy (ARP/ARR)	F1-score	Top-10 Accuracy	Power Consumption	Hardware Complexity	Remarks
Conventional Gabor + KNN	0.70 – 0.75	0.72	0.90	> 1.5 W	High (multipliers)	Accurate but not power-efficient
DGWFB + Standard KNN	0.78 – 0.81	0.80	0.95	~0.50 W	Medium (shift-and-add)	Efficient but limited by Euclidean distance
Proposed DGWFB + Hybrid KNN	**0.8163**	**0.8163**	**0.9943**	**0.50 – 0.52 W**	Low (clock-gated, shift-and-add)	Best trade-off: high accuracy + low power

6. Conclusion and Future Scope

In this work, a **Hybrid KNN and Dyadic Gabor Wavelet Filter Bank (DGWFB)**-based architecture was proposed for **power-efficient VLSI-based medical image retrieval**. The DGWFB module, implemented in Verilog, enabled **multiplier-less feature extraction** using shift-and-add logic, making it highly suitable for hardware realization. A **Hybrid KNN classifier** was employed to enhance retrieval accuracy by combining **Euclidean distance** and **Cosine similarity** with adaptive weighting. The integration of MATLAB for preprocessing and classification with Verilog for DGWFB hardware ensured a complete **hardware-software co-design** solution.
Experimental results demonstrated that the proposed system achieves a strong balance between **accuracy, speed, and hardware efficiency**:

- **Retrieval accuracy**: ARP and ARR of ~0.8163, Top-10 accuracy of 99.43%, and F1-score of 0.8163 across the 4-class MRI dataset.

- **Hardware efficiency**: FPGA synthesis reports indicated **low LUT/FF utilization**, only **5–8% DSP usage**, and a total **power consumption of ~0.50 W**, confirming suitability for **portable medical applications**.
- **Comparative analysis**: The proposed system outperformed both conventional Gabor + KNN and DGWFB + standard KNN, proving its ability to combine **high retrieval accuracy with low power consumption**.

Overall, the proposed framework offers a **reliable, scalable, and energy-aware solution** for next-generation medical image retrieval systems.

Future Scope

While the results are promising, several directions can further enhance the system:

- **Dataset Expansion:** Extending evaluation to larger and more diverse medical datasets (CT, PET, Ultrasound) to validate generalization.
- **Deep Feature Integration:** Combining DGWFB features with **CNN-based embeddings** could yield a hybrid deep learning–VLSI pipeline for improved retrieval accuracy.
- **On-Chip Classification:** Implementing Hybrid KNN entirely in FPGA/VLSI, reducing dependency on MATLAB, for a complete hardware-based retrieval system.
- **Low-Power Optimizations:** Techniques such as **approximate computing, dynamic voltage scaling, and memory compression** can further reduce energy consumption.
- **Edge/IoT Deployment:** The framework can be extended to **wearable or portable diagnostic devices**, enabling real-time decision support in rural healthcare and telemedicine.

Thus, the proposed Hybrid KNN + DGWFB framework serves as a **foundation for future medical imaging systems**, bridging the gap between algorithmic innovation and practical hardware implementation.

7. REFERENCES

[1] C. Li, G. Duan, and F. Zhong, "Rotation invariant texture retrieval considering the scale dependence of Gabor wavelet," *IEEE Trans. Image Process.*, vol. 24, no. 8, pp. 2344–2354, Aug. 2015.
[2] W. Gu, C. Xiang, Y. V. Venkatesh, D. Huang, and H. Lin, "Facial expression recognition using radial encoding of local Gabor features and classifier synthesis," *Pattern Recognit.*, vol. 45, no. 1, pp. 80–91, 2012.
[3] H. Kasban, "Fingerprints verification based on their spectrum," *Neurocomputing*, vol. 171, pp. 910–920, Jan. 2016.
[4] S. Jia, K. Wu, J. Zhu, and X. Jia, "Spectral-spatial Gabor surface feature fusion approach for hyperspectral imagery classification," *IEEE Trans. Geosci. Remote Sens.*, vol. 57, no. 2, pp. 1142–1154, Feb. 2019.
[5] S. A. A. Shah, A. Shahzad, M. A. Khan, C.-K. Lu, and T. B. Tang, "Unsupervised method for retinal vessel segmentation based on Gabor wavelet and multiscale line detector," *IEEE Access*, vol. 7, pp. 167221–167228, 2019.
[6] S. Marcelja, "Mathematical description of the responses of simple cortical cells," *J. Opt. Soc. Amer.*, vol. 70, no. 11, pp. 1297–1300, Nov. 1980.
[7] L. Wiskott, J.-M. Fellous, N. Kuiger, and C. von der Malsburg, "Face recognition by elastic bunch graph matching," *IEEE Trans. Pattern Anal. Mach. Intell.*, vol. 19, no. 7, pp. 775–779, Jul. 1997.
[8] I. Sertcelik, O. Kafadar, and C. Kurtulus, "Use of the two dimensional Gabor filter to interpret magnetic data over the Marmara Sea, Turkey," *Pure Appl. Geophys.*, vol. 170, no. 5, pp. 887–894, 2013.
[9] J.-K. Kamarainen, V. Kyrki, and H. Kalviainen, "Invariance properties of Gabor filter-based features—Overview and applications," *IEEE Trans. Image Process.*, vol. 15, no. 5, pp. 1088–1099, May 2006.
[10] B. S. Manjunath and W. Y. Ma, "Texture features for browsing and retrieval of image data," *IEEE Trans. Pattern Anal. Mach. Intell.*, vol. 18, no. 8, pp. 837–842, Aug. 1996.
[11] S. Qian and D. Chen, "Discrete Gabor transform," *IEEE Trans. Signal Process.*, vol. 41, no. 7, pp. 2429–2438, Jul. 1993.
[12] X. Gao, F. Sattar, and R. Venkateswarlu, "Multiscale corner detection of gray level images based on log-Gabor wavelet transform," *IEEE Trans. Circuits Syst. Video Technol.*, vol. 17, no. 7, pp. 868–875, Jul. 2007.
[13] N. Ranganathan, R. Mehrotra, and K. R. Namuduri, "An architecture to implement multiresolution," in *Proc. ICASSP*, vol. 2, 1991, pp. 1157–1160.
[14] S. Qiu, F. Zhou, and P. E. Crandall, "Discrete Gabor transforms with complexity O(NlogN)," *Signal Process.*, vol. 77, no. 2, pp. 159–170, Sep. 1999.
[15] O. Nestares, R. F. Navarro, J. Portilla, and A. Tabernero, "Efficient spatial-domain implementation of a multiscale image representation based on Gabor functions," *J. Electron. Imag.*, vol. 7, no. 1, pp. 166–173, 1998.
[16] I. T. Young, L. J. V. Vliet, and M. V. Ginkel, "Recursive Gabor filtering," *IEEE Trans. Signal Process.*, vol. 50, no. 11, pp. 2798–2805, Nov. 2002.
[17] A. Bernardino and J. Santos-Victor, "Fast IIR isotropic 2-D complex Gabor filters with boundary initialization," *IEEE Trans. Image Process.*, vol. 15, no. 11, pp. 3338–3348, Nov. 2006.
[18] E. Cesur, N. Yildiz, and V. Tavsanoglu, "On an improved FPGA implementation of CNN-based Gabor-type filters," *IEEE Trans. Circuits Syst. II*, vol. 59, no. 11, pp. 815–819, Nov. 2012.
[19] G. D. Licciardo, C. Cappetta, and L. Di Benedetto, "Design of a Gabor filter HW accelerator for applications in medical imaging," *IEEE Trans. Compon. Packag. Manuf. Technol.*, vol. 8, no. 7, pp. 1187–1194, Jul. 2018.
[20] E. Painkras and C. Charoensak, "A VLSI architecture for Gabor filtering in face processing applications," in *Proc. Int. Symp. Intell. Signal Process. Commun. Syst.*, 2005, pp. 437–440.

[21] G. G. C. Lee, Z.-J. Huang, C.-Y. Chen, and C.-F. Chen, "Implementation of Gabor feature extraction algorithm for electrocardiogram on FPGA," in *Proc. ISCAS*, 2015, pp. 798–801.
[22] N. Onizawa, D. Katagiri, K. Matsumiya, W. J. Gross, and T. Hanyu, "Gabor filter based on stochastic computation," *IEEE Signal Process. Lett.*, vol. 22, no. 9, pp. 1224–1228, Sep. 2015.
[23] A. M. Anbaran, P. Torkzadeh, R. Ebrahimpour, and N. Bagheri, "Modification and hardware implementation of cortex-like object recognition model," *IET Image Process.*, vol. 14, no. 14, pp. 3490–3498, 2020.
[24] V. Dakshayani, G. R. Locharla, P. Plawiak, V. Datti, and C. Karri, "Design of a Gabor filter-based image denoising hardware model," *Electronics*, vol. 11, no. 7, pp. 1063–1078, 2022.
[25] T. Andrysiak and M. Choraś, "Image retrieval based on hierarchical Gabor filters," *Int. J. Appl. Math. Comput. Sci.*, vol. 15, no. 4, pp. 471–480, 2005.
[26] J. P. Jones and L. A. Palmer, "An evaluation of the two-dimensional Gabor filter model of simple receptive fields in cat striate cortex," *J. Neurophysiol.*, vol. 58, no. 6, pp. 1233–1258, Dec. 1987.
[27] J. Ilonen, J. K. Kamarainen, and H. Kalviainen, "Fast extraction of multiresolution Gabor features," in *Proc. ICIAP*, Sep. 2007, pp. 481–486.
[28] A. K. Samantaray and A. D. Rahulkar, "New design of adaptive Gabor wavelet filter bank for medical image retrieval," *IET Image Process.*, vol. 14, no. 4, pp. 679–687, Mar. 2020.
[29] P. Lo et al., "Extraction of airways from CT (EXACT'09)," *IEEE Trans. Med. Imag.*, vol. 31, no. 11, pp. 2093–2107, Nov. 2012.
[30] D. S. Marcus, T. H. Wang, J. Parker, J. G. Csernansky, J. C. Morris, and R. L. Buckner, "Open access series of imaging studies (OASIS): Cross-sectional MRI data," *J. Cognit. Neurosci.*, vol. 19, no. 9, pp. 1498–1507, Sep. 2007.
[31] A. Kumar and B. Raman, "Power-Efficient VLSI Architecture of a New Class of Dyadic Gabor Wavelets for Medical Image Analysis," *IEEE Trans. Biomed. Circuits Syst.*, vol. 14, no. 6, pp. 1195–1206, 2020.
[32] T. Cover and P. Hart, "Nearest Neighbor Pattern Classification," *IEEE Trans. Inf. Theory*, vol. 13, no. 1, pp. 21–27, 1967.
[33] R. Duda, P. Hart, and D. Stork, *Pattern Classification*, 2nd ed., Wiley, 2000.
[34] Xilinx Inc., "Vivado Design Suite User Guide," 2023. [Online]. Available: https://www.xilinx.com
[35] Kaggle, "Brain MRI Images for Brain Tumor Detection Dataset," 2023. [Online]. Available: https://www.kaggle.com/navoneel/brain-mri-images-for-brain-tumor-detection
[36] National Electrical Manufacturers Association (NEMA), "NEMA Medical Imaging Dataset," 2023. [Online]. Available: https://www.nema.org/medical-imaging
[37] Brain Tumor MRI Dataset (Glioma, Meningioma, Pituitary, No Tumor), 2023. [Online]. Available: https://www.kaggle.com/sartajbhuvaji/brain-tumor-classification-mri
[38] M. R. Hemanth, C. C. Sekhar, "FPGA Implementation of Image Processing Algorithms for Real-Time Medical Systems," *Int. J. VLSI Design*, vol. 9, no. 3, pp. 45–52, 2021.
[39] L. Xu, W. Lin, and C.-C. J. Kuo, *Visual Quality Assessment by Machine Learning*. Singapore: Springer, 2015.
[40] A. Teuner and B. J. Hosticka, "Adaptive filter for two-dimensional Gabor transformation and its implementation," *IEE Proc. I (Commun., Speech Vis.)*, vol. 140, no. 1, pp. 2–6, 1993.